ChemComm

Accepted Manuscript

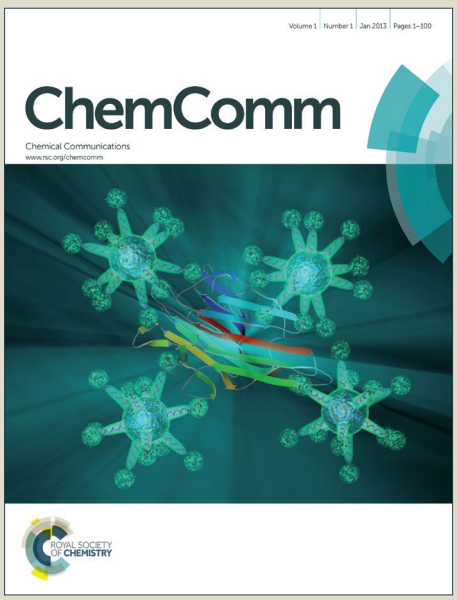

This is an *Accepted Manuscript*, which has been through the Royal Society of Chemistry peer review process and has been accepted for publication.

Accepted Manuscripts are published online shortly after acceptance, before technical editing, formatting and proof reading. Using this free service, authors can make their results available to the community, in citable form, before we publish the edited article. We will replace this *Accepted Manuscript* with the edited and formatted *Advance Article* as soon as it is available.

You can find more information about *Accepted Manuscripts* in the Information for Authors.

Please note that technical editing may introduce minor changes to the text and/or graphics, which may alter content. The journal's standard Terms & Conditions and the Ethical guidelines still apply. In no event shall the Royal Society of Chemistry be held responsible for any errors or omissions in this *Accepted Manuscript* or any consequences arising from the use of any information it contains.

ROYAL SOCIETY OF CHEMISTRY

www.rsc.org/chemcomm

Please do not adjust margins

ChemComm

COMMUNICATION

Ambipolar organic field-effect transistor based on an AIE-active single crystal with high mobility level of 2.0 cm^2 V^{-1} s^{-1}

Received 00th January 20xx,
Accepted 00th January 20xx

DOI: 10.1039/x0xx00000x

www.rsc.org/

*Jian Deng[a], Yuanxiang Xu[a], Liqun Liu[a], Cunfang Feng[a], Jia Tang[a], Yu Gao[a], Yan Wang[a] *, Bing Yang[a] , Ping Lu[a], Wensheng Yang[a], and Yuguang Ma[a,b] **

The organic field-effect transistors (OFETs) based on an aggregation-induced emission (AIE) material were fabricated with calcium-gold asymmetric electrodes system. The devices showed very high and balanced mobility, reaching 2.50 and 2.10 cm^2 V^{-1} s^{-1} respectively for electron and hole. The strong green electroluminescence from the single-crystal side edge was observed from all the devices. This work demonstrates that AIE active materials could not only achieve high luminescence, but also be used in light emitting transistors and achieve very high mobility.

Aggregation-induced emission (AIE) is the photophysical phenomenon that some luminescence species suffer very low emission efficiency in the dilute solution but high luminescence efficiency in solids.[1-4] This phenomenon is firstly proposed by Tang and his co-workers from 1-methyl-1,2,3,4,5-pentaphenylsilole.[3] After several years of development, the AIE-active materials have been widely studied for their potential applications in organic light-emitting diodes (OLEDs) and organic field-effect transistors (OFETs).[5-9] In order to meet the requirements of the applications in the high performance organic photoelectric devices, it's vital for the AIE active organic semiconductors to obtain high luminescence efficiency and high carrier mobility. The AIE active molecules have abundant relative flexible chemical bonds, which endure the molecule with numerous configurations. In the dilute solutions, the excitons can be easily quenched by the vibration and rotation of the groups. However, the quenching processes are severely restricted by the strong intermolecular forces in the aggregation state, which result in the high emission efficiency in the solid. Despite the high luminescence, the carrier mobility from reported AIE active materials are very low, typically in the level of 10^{-6}~10^{-1} cm^2 V^{-1} s^{-1},[10, 11] due to the distorted molecular conformation and weak π-π staking in the solid. To achieve high carrier mobility, the compact π-π staking between the π-conjugated molecules and polymers, typically H-aggregation, is needed. Yet such a stacking model often gives rise to the non-radiation process due to the optical forbidden transition, which decreases the luminescence efficiency in the solid phase dramatically. Some strategies, including enlarging the molecule distance and forming the X-aggregation or J-aggregation by controlling the dipole-dipole interaction,[12-14] have been employed to improve the solid luminescence. Among them, the J-aggregation is thought to be the balanced strategy to achieve both high mobility and high luminescence for organic crystals, since the stacking model has excellent π-orbital overlapping which is a vital factor during the charge transport,[15-17] and the impressive allowed electronic transition. For AIE active molecules, the flexible chemical bonds make it possible for the organic semiconductors to adjust the molecular conformation and packing model by introducing some strong intermolecular force, such as π-π interaction and hydrogen bonds.

Trans-1,4-distyrylbenzene (trans-DSB) is a typical aggregation-caused quenching (ACQ) material.[18] By introducing the cayno groups, the target molecule, 1,4-bis(2-cyano-2-phenylethenyl)benzene (β-CNDSB) becomes an AIE active substance (**Figure 1a**).[19] In the dilute solution, the β-CNDSB shows a twist conformation (**Figure 1b**) and very weak fluorescence. By carefully controlling the grown condition, the green slice like single-crystals were obtained by the method of physical vapour transport (PVT).[20] In the green single crystals, the molecule exhibits nearly planar conformation (**Figure 1c-d**) and J-aggregation, resulting in the high luminescent efficiency. The formation of the 2-dimensional single crystal are thought to be driven by the strong π-π interactions and multiple hydrogen bonds. Strong emission can be observed from the edge of the

[a] State Key Laboratory of Supramolecular Structure and Materials, College of Chemistry, Jilin University, Changchun, 130012, P. R. China.
[b] State Key Laboratory of Luminescent Materials and Devices, South China University of Technology, Guangzhou, 510640, P. R. China.
* E-mail: wangy2011@jlu.edu.cn, ygma@jlu.edu.cn

Electronic Supplementary Information (ESI) available: Experimental Section, Synthetic route, additional characteristics of the OFETs, Statistics of the devices' mobility, comparison of carrier mobility with other AIE crystals, movie of the edge emission when devices operating, structure of the single-crystals, the calculated S0–S1 transition dipole moment. See DOI: 10.1039/x0xx00000x

ChemComm Accepted Manuscript

Please do not adjust margins

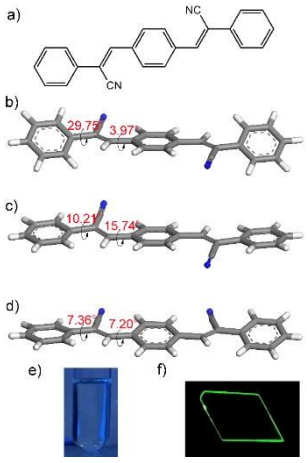

Figure 1. a) Chemical structure of β-CNDSB. b) Molecular conformation in the dilute solutions, calculated by Gaussian 0.9. D. 01.[21] c,d) Molecular conformations in the green crystal. e) The β-CNDSB dilute solution didn't show any megascopic fluorescent when excited by UV lamp (solvent, dichloromethane). f) Green light emits from the side edge of the crystal when excited by 365 nm UV lamp.

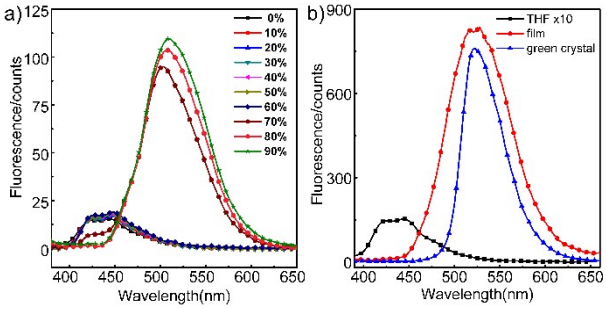

Figure 2. Emission spectra of β-CNDSB in serials of environments. a) Light emission of β-CNDSB in the water/THF mixed solvent. The concentration of the β-CNDSB in the solution was fixed at 3.0 x 10^{-5} M. The labels stand for the percentage of water in the solvent. b) Light emission of β-CNDSB when dissolve in THF, spin-coating film (thickness 100 nm) and slice like green single-crystal.

crystals when excited by a 365-nm UV lamp (**Figure 1f**). In addition, the planar conformation and J-aggregation are very propitious to achieve high carrier mobility. The investigations about the carrier transport behaviours of the β-CNDSB single crystals are lack in the previous reports but very important to explore the AIE materials with high luminescence efficiency and high carrier mobility. The OFETs are the proper physical prototype to investigate carrier transport behaviour of organic semiconductors. In this paper, the AIE-active β-CNDSB single-crystals were used to fabricate OFETs and the property of carrier transport was analysed in detail. The devices were demonstrated the high mobility level of more than 2.0 $cm^2 V^{-1} s^{-1}$, which is at least one order higher than the reported mobility in the OFETs based on the AIE active materials.

In the THF solution, the β-CNDSB exhibits typical AIE characteristics, shown in **Figure 2a**. When dissolved in the dilute solution, the β-CNDSB shows very weak emission with two peaks around 421 nm and 448 nm. In this condition, the β-CNDSB completely dissolve in the solvent as isolated state (**Figure 1b**) and there exist nearly no interaction between the molecule. The twist conformation limits the conjugate efficiency of the molecule. In addition, the relatively flexible ethylene bonds make it very easy to consume the energy of the excitons. As a result, the solution exhibits weak blue emission. When the water's percentage reach 70%, the two weak emission peaks decrease to less than half of the strength in the pure THF solution. At the same time, there grow up one strong emission band with the peak at 503 nm. The result suggests the β-CNDSB may exist as two state, the isolated state and the aggregation state. In the aggregation state, the strong molecular interaction force the molecule take use the more planarity conformation and limits the vibration and rotation of the flexible bonds. Consequently, there emerges the strong emission band around 503 nm. In the 80% and 90% solutions, the emission bands around 421~448 nm have complete disappeared and the enhancement emission bands shift to around 508 nm, suggesting the isolate state has not existed any more. In the slice-like single crystals, the strong green light with the peak around 520 nm (**Figure 2b**) mainly emits from the side edge of the crystals (**Figure 1f**). The photoluminescence efficiency was measured by an integrating sphere when excited by 365 nm UV light, which shows the photoluminescence yield (η_{pl}) up to 75%.

For the β-CNDSB single-crystal, the simultaneous injection and transportation of both electron and holes had been obtained from the OFETs with symmetric gold electrodes in our previous work. However, the electro-driven light emission has not been observed from the devices. The high injection barrier between the lowest unoccupied molecular orbital (LUMO) level and work function of Au may seriously limit the electron density in the channel. In order to reduce the injection barrier for electron, and keep the high hole injection efficiency, the OFETs with calcium/gold asymmetric electrodes geometry was employed here, shown in **Figure 3a**.

In the present work, the typical out-put characters of N-channel were shown in Figure 3c. Comparing with the devices using Au symmetric electrodes configuration (**Figure 3b**), the Ca's work function (-2.87 eV) lies closer to the LUMO level of β-CNDSB (-3.26 eV). As the result, the accumulated threshold voltage for the N-channel in these devices reduces from more than 30 V in the symmetric gold electrodes system to less than 20 V when the asymmetric Ca-Au electrodes system was employed (Figure S2). Though the energy map suggest it might be ohmic contact in the crystal/metal interface, the curves show nonlinear I-V relation as the source-drain voltage (V_{ds}) is low, which indicate there still exist some injection barrier. This barrier may result from the slightly oxidized of the calcium during the storage and trace quantities of oxygen when deposition. Though the evaporation chamber had been pumped to a very low pressure ($<1\times10^{-4}$) before the calcium deposition, there may still exist trace amounts of oxygen atoms. These oxygen atoms create some CaO traps in the interface of calcium and the β-CNDSB single crystal.[22] In the device with 100 μm channel width, the maximum drain current (I_d) in the out-put curves reached 2.0 uA when the gate voltage (V_g) was set at 140 V. Benefitted from the better energy match, the maximum current density rises from 90.7 A/cm^2 in the symmetric gold electrodes system to 200

ChemComm Accepted Manuscript

This journal is © The Royal Society of Chemistry 20xx

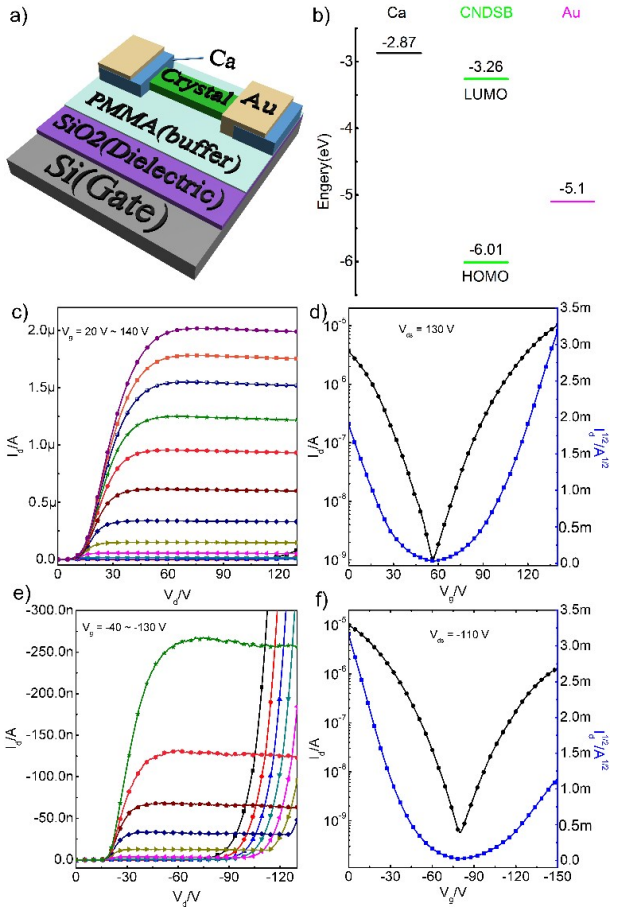

Figure 3. OFETs characteristic of the devices based on the green β-CNDSB single-crystals, channel with: 100 um, channel length: 50 um. (a) Schematic representation of the β-CNDSB single-crystal device. (b) Energy level diagram of β-CNDSB, comparing with Au and Ca's work function. The energy level are measured by the method of Cyclic Voltammetry. (c) Out-put characters of N-channel. (d) Transfer character of N-channel, black line: $(I_d)^{1/2}$, blue line: I_d. (e) Out-put character of P-channel. (f) Transfer character of P-channel, blue line: $|I_d|^{1/2}$, black line: $|I_d|$.

A/cm². Noting that, the calculations of the current density here are all based on the assumption that the thickness of the accumulate layer is 10 nm[23]. At low positive V_g and high V_{ds}, the current showed a pronounced increase as the V_{ds} increasing, which is a typical characteristic for ambipolar transistors. In order to protect the electrodes from damaged, the V_{ds} was limited to 130 V. As a result of that, the obvious hole transport can be observed under relative low V_g (40~80 V). In the hole enhancement model, as the energy mismatch between the highest occupied molecular orbital (HOMO) and gold work function, the out-put curves exhibit typical Schottky contact, which can be inferred from the nonlinear increased current at low V_{ds} (See **Figure 3e**). When the V_{ds} is high, the ambipolar characters are much more obvious. Though the V_g was set as -100 V, the electron transport can still be observed from the channel as the V_{ds} is biasing more negative than -125 V. The maximum out-put current reach 270 nA as the V_g was set at -130 V.

The transfer characteristics were demonstrated in both N-enhancement and P-enhancement model, shown respectively in the **Figure 3d** and **Figure 3f**. The transfer curves show very close slope, which indicates the carrier mobility are well balanced. When the V_{ds} is low, the potential for hole and electron injection can't exceed the threshold voltage simultaneously. As a result, only one carrier can accumulate and the devices work in unipolar model. In the condition, the transistors exhibit very high $I_{on/off}$ ratio, typically higher than 10^5 (**Figure S3**). In addition, the transfer curves of N-channel and P-channel show similar hysteresis when the devices were scanned forward and backward in a short time (**Figure S4**). The measurement of the gate current (I_g) shows the leakage current reaches around 100 nA when V_g= 120 V (**Figure S5**), which may result in the distortion of the transfer curves under low V_{ds}. The ambipolar behaviours were observed from all the working devices when the transistors operated under slight higher V_{ds} (e.g. > 40 V). During the sweeping of V_g, the maximum I_d when the recombination of the electron and hole was observed higher than 74 nA when the electron and hole completely combine in a device with the channel width of 180nm and length of 70 nm (**Figure S6**). For most of the reported organic single crystals with ambipolar characteristics, the transistors always need relatively high operation voltage for the two opposite carriers to inject and transport simultaneously as they usually suffer from very high threshold voltage for electron (e.g. for BP3T, $V_{g,th}$(electron) > 120 V[24]). Though the capacity of the substrate used here is 0.85 times higher than the capacity in the reported OFETs, the devices shows more than 3 times lower $V_{g,th}$ for electron (10~30 V). Herein, the β-CNDSB single crystal has evidently reduced the working voltage of ambipolar OFETs. The slopes of $I_d^{1/2}$-V_g in the saturated regimes were calculated, and then were used to calculate the carrier mobility. The results showed that the highest electron and hole mobility of 2.50 and 2.10 $cm^2\ V^{-1}\ s^{-1}$, respectively. Among the 26 working devices (**Figure S7**), the average mobility is 0.526 and 0.232 $cm^2\ V^{-1}\ s^{-1}$ for electron and hole, respectively. As the previous work had explained, the J-aggregation and highly ordered multiple

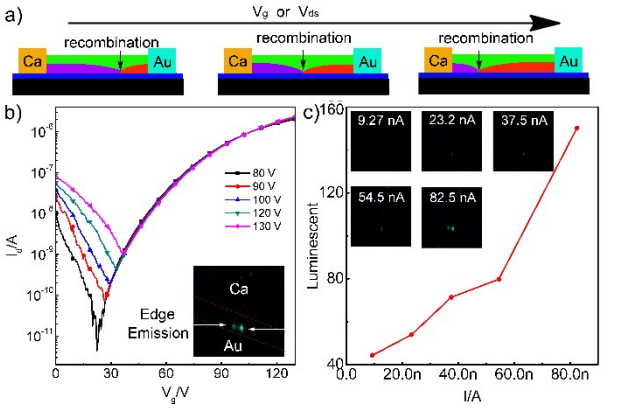

Figure 4. a) Schematic diagram of the recombination zone's shift when the V_g or V_{ds} increase. b) I_d-V_g characteristic of an OFET device with Ca-Au asymmetric electrodes during the electroluminescence test. Insert: the light emission in the device channel (V_{ds}=130 V). c) Emission brightness of the OFET device, derived from the captured images when the device worked under the different I_d. The luminescent intensity (Y-axis) is calculated from the captured figures during the devices operating. The I_d was calculated by the out-put curves with different V_g. Insert: electroluminescence images taken under serials of I_d. The exposure time of the CCD camera while devices operation is set at 588 ms to obtain the clear image.

ChemComm Accepted Manuscript

hydrogen bonds are very helpful to achieve high mobility for the organic single crystals. To the best of our knowledge, it is the highest carrier mobility for the reported AIE active materials (**Table S1**).

In ambipolar OFETs, the electron and hole can simultaneously inject into the active materials by biasing the V_g or V_d. In the current work, we scanned the V_g positively with serials of fixed V_{ds}. when the V_{ds} is relative high (e.g. 40 V), both the opposite carriers can be accumulated within the channel. This process induces the p-n junction who leads to the recombination of the electron and hole, called ambipolar work model. When the V_d increase further, the recombination zone will move towards the source electrodes slightly as the injection of the hole become stronger (**Figure 4a**).

In this device, clear green emission from the side edge of the crystal was observed, and nearly no emission can be found in crystal surface, as shown in the inset of **Figure 4b**. And the electroluminescence becomes stronger with increase of the I_d, shown in **Figure 4c**. Besides, the luminescent brightness increases slightly faster with accumulated current raising. However, the shift of the recombination zone isn't observed clearly as the current imaging system is short of resolution. The electroluminescent spectrums were absent in our current experiment as lack of the focus system to collect the emission light from the device into the detector of fiber optic spectrometer. Nonetheless, after calibrating the colour of the imaging system using the green β-CNDSB single crystals under UV light, the Commission Internationale de L'Eclairage (CIE) coordinates of the electroluminescence is (0.286, 0.551).

In our previous work, the crystal structure and facets had been carefully investigated. The details are listed in the **Supporting Information** part 9 and **Figure S8**. The result shows the crystal's surfaces were formed by the layer-by-layer structure. In addition, the theoretical calculation demonstrates the orientation of the S0–S1 transition dipole moment of β-CNDSB lies along the molecular long axis, shown in **Figure S9**, indicating the light emission would propagate along the short axis and perpendicular to the molecular plane. That means the light should be emitted in all directions within the crystal plane from the source in the recombination zone. However, the light propagate along the channel would been completely absorbed by the electrodes when the crystal thicker than the electrodes. The other portion of the emission light could still propagate to all the crystal edges. As the result of that, the observed light spot indicated the approximate position of the recombination zone.

In summary, series of OFETs based on the AIE active single crystals were investigated. The ambipolar mobility were demonstrated as high as 2.50 and 2.10 $cm^2 V^{-1} s^{-1}$ for electron and hole, respectively. The results show that the high luminescent efficiency and high carrier mobility can be achieved simultaneously by carefully design and control the molecular conformation. The strong green electroluminescence from the single-crystal side edge was observed from all the devices. This work also demonstrates that AIE active materials could not only achieve high luminescence, but also be used in light emitting transistors and achieve very high mobility.

This work was supported by National Science Foundation of China (NFSC) (Grant No. 51103054, 51273076, 91233113) and Ministry of Science and Technology of China (Grant No. 2013CB834705).

Notes and references

1 J. W. Chen, B. Xu, X. Y. Ouyang, B. Z. Tang and Y. Cao, *J. Phys. Chem. A*, 2004, **108**, 7522-7526.
2 S. Jang, S. G. Kim, D. Jung, H. Kwon, J. Song, S. Cho, Y. C. Ko and H. Sohn, *Bull. Korean Chem. Soc.*, 2006, **27**, 1965-1966.
3 J. D. Luo, Z. L. Xie, J. W. Y. Lam, L. Cheng, H. Y. Chen, C. F. Qiu, H. S. Kwok, X. W. Zhan, Y. Q. Liu, D. B. Zhu and B. Z. Tang, *Chem. Commun.*, 2001, DOI: 10.1039/b105159h, 1740-1741.
4 H. Tong, Y. Q. Dong, M. Haussler, J. W. Y. Lam, H. H. Y. Sung, I. D. Williams, J. Z. Sun and B. Z. Tang, *Chem. Commun.*, 2006, DOI: 10.1039/b515798f, 1133-1135.
5 J. W. Park, S. Nagano, S. J. Yoon, T. Dohi, J. Seo, T. Seki and S. Y. Park, *Adv. Mater.*, 2014, **26**, 1354-1359.
6 S. Yagai, S. Okamura, Y. Nakano, M. Yamauchi, K. Kishikawa, T. Karatsu, A. Kitamura, A. Ueno, D. Kuzuhara, H. Yamada, T. Seki and H. Ito, *Nat. Commun.*, 2014, **5**.
7 M. S. Yuan, D. E. Wang, P. C. Xue, W. J. Wang, J. C. Wang, Q. Tu, Z. Q. Liu, Y. Liu, Y. R. Zhang and J. Y. Wang, *Chem. Mater.*, 2014, **26**, 2467-2477.
8 S. K. Park, S. Varghese, J. H. Kim, S. J. Yoon, O. K. Kwon, B. K. An, J. Gierschner and S. Y. Park, *J. Am. Chem. Soc.*, 2013, **135**, 4757-4764.
9 H. Nakanotani, M. Saito, H. Nakamura and C. Adachi, *Appl. Phys. Lett.*, 2009, **95**, 033308-033303.
10 G. Mu, W. Zhang, P. Xu, H. Wang, Y. Wang, L. Wang, S. Zhuang and X. Zhu, *J. Phys. Chem. C*, 2014, **118**, 8610-8616.
11 Z. J. Zhao, Z. F. Li, J. W. Y. Lam, J. L. Maldonado, G. Ramos-Ortiz, Y. Liu, W. Z. Yuan, J. B. Xu, Q. Miao and B. Z. Tang, *Chem. Commun.*, 2011, **47**, 6924-6926.
12 T. Főrster, *Discuss. Faraday Soc.*, 1959, **27**, 7-17.
13 M. Kasha, H. R. Rawls and E.-B. M. Ashraf, *Pure Appl. Chem.*, 1965, **11**, 371-392.
14 Z. Xie, B. Yang, F. Li, G. Cheng, L. Liu, G. Yang, H. Xu, L. Ye, M. Hanif, S. Liu, D. Ma and Y. Ma, *J. Am. Chem. Soc.*, 2005, **127**, 14152-14153.
15 J.-L. Brédas, D. Beljonne, V. Coropceanu and J. Cornil, *Chem. Rev.*, 2004, **104**, 4971-5003.
16 R. A. Marcus, *J. Chem. Phys.*, 1956, **24**, 966.
17 S. Yin, Y. Yi, Q. Li, G. Yu, Y. Liu and Z. Shuai, *J. Phys. Chem. A*, 2006, **110**, 7138-7143.
18 Z. Q. Xie, W. J. Xie, F. Li, L. L. Liu, H. Wang and Y. G. Ma, *J. Phys. Chem. C*, 2008, **112**, 9066-9071.
19 C. W. Chang, C. J. Bhongale, C. S. Lee, W. K. Huang, C. S. Hsu and E. W. G. Diau, *J. Phys. Chem. C*, 2012, **116**, 15146-15154.
20 J. Deng, J. Tang, Y. Xu, L. Liu, Y. Wang, Z. Xie and Y. Ma, *Phys. Chem. Chem. Phys.*, 2015, **17**, 3421-3425.
21 Gaussian, Gaussian, Inc., , Wallingford CT **2009**.
22 S. Z. Bisri, T. Takenobu, T. Takahashi and Y. Iwasa, *Appl. Phys. Lett.*, 2010, **96**, 183304.
23 H. Wang, J. Wang, H. Huang, X. Yan and D. Yan, *Org. Electron.*, 2006, **7**, 369-374.
24 S. Z. Bisri, T. Takenobu, Y. Yomogida, H. Shimotani, T. Yamao, S. Hotta and Y. Iwasa, *Adv. Funct. Mater.*, 2009, **19**, 1728-1735.

ChemComm Accepted Manuscript

This journal is © The Royal Society of Chemistry 20xx